Astron. Astrophys. 253, 35–48 (1992)

ASTRONOMY AND ASTROPHYSICS

The soft X-ray excess in Einstein quasar spectra

J.L. Masnou[1,*], B.J. Wilkes[2,], M. Elvis[2], J.C. McDowell[2,***], and K.A. Arnaud[3,****]**

[1] UPR176, DARC, Observatoire de Paris, Section de Meudon, 5, Place Jules Janssen, F-92195 Meudon, France
[2] Harvard-Smithsonian Center for Astrophysics, 60, Garden St., Cambridge, MA 02138, USA
[3] NASA/Goddard Space Flight Center, Greenbelt, MD 20771, USA

Received January 2, accepted May 13, 1991

Abstract. We study the low-energy excess above a high-energy power law in the X-ray spectra for a signal-to-noise limited, subsample of 14 quasars from the Wilkes & Elvis (1987) sample. Detailed analysis of the Einstein imaging proportional counter (IPC) data, combined with monitor proportional counter (MPC) data where possible, and the use of accurate Galactic N_H values allow us to estimate the flux of any detected excess and improve constraints on the spectral parameters at higher (>0.6 keV) X-ray energies. We find a significant excess in 8 of the 14 objects, confined in all but one case to below 0.6 keV. The excess is typically strong, dominating the $\lesssim 0.3$ keV X-ray flux and being 1–6 times as strong as the high-energy component at 0.2 keV. In 3C273, multiple observations show that the excess is variable. The lack of spectral information, uncertainty in the intrinsic line-of-sight absorption and the possibility of variation prevents the detection of any relation with the optical/ultraviolet blue bump. Comparison with an existing accretion disk model for the blue bump suggests that, for this model to explain both the blue bump and the soft X-ray excess, a range of disk parameters are required to explain the whole sample.

Key words: quasars – X-rays: spectroscopy – X-rays: general

1. Introduction

Recent soft X-ray observations have shown that active galactic nuclei (AGN) and quasars commonly show strong excess emission above the extrapolation of their higher-energy slopes (Singh et al. 1985; Arnaud et al. 1985; Branduardi-Raymont et al. 1985; Wilkes & Elvis 1987; Turner & Pounds 1989; Elvis et al. 1991a). These excesses occur primarily in the C-band, i.e. below the 0.28 keV carbon edge, and rise steeply to lower energies. Information is generally limited to a single discrepant point at low energies when compared to the slope at higher energies (1–10 keV) (e.g. Turner & Pounds 1989). In this paper we use the highest signal-to-noise imaging proportional counter (IPC) observations from the Wilkes & Elvis (1987) quasar sample, combined with higher-energy (2–10 keV) monitor proportional counter (MPC) data where it is useful, to give data extending from 0.1–1.0 keV. These data, combined with accurate Galactic N_H values (Elvis et al. 1989), allow two-component spectral fits, and, thus, a well-constrained estimate of the observed flux in the soft excess.

Although there are viable alternatives, such as free–free emission (Barvainis 1990; Ferland et al. 1990), the optical/ultraviolet (UV) blue bump is generally modeled as thermal emission from an accretion disk possessing a range of temperatures (Shields 1978; Malkan & Sargent 1982), an interpretation which is enticing both observationally and theoretically. An obvious identification of the soft X-ray excess is then the high-energy tail of the thermal emission (Arnaud et al. 1985; Bechtold et al. 1986; Pounds et al. 1986; Czerny & Elvis 1987). In this case it would originate in the hottest material, at the innermost edge of the accretion disk at ~ 10 Schwarzschild radii. Should this be confirmed, the excess will provide far stronger constraints on the physical conditions of this part of the disk than have been possible so far. Quantitative measurement of the soft excess is thus of considerable importance.

2. Analysis

2.1. The data

We have selected the highest signal-to-noise observations in the Wilkes & Elvis (1987) sample of quasars observed with Einstein IPC, those with $\gtrsim 1200$ net counts. This yielded a subset of 14 quasars, 5 of which are radio-loud (radio-loudness, $R_L > 1.0$, Wilkes & Elvis 1987). Details of the X-ray observations along with redshift and Galactic column density of neutral hydrogen are given in Table 1. PG 1211+143, which is a member of the sample, is included for completeness in the discussion although it is not reanalyzed here. We include two additional observations of 3C273 not reported by Wilkes & Elvis (1987). For completeness and comparison with the earlier results, the results of single power law fits with free N_H to the IPC data alone for these two observations, using Brown & Gould (1970) absorption coefficients, are given in Table 2a and Fig. 1. Throughout the remainder of our analysis, absorption coefficients are taken from Morrison & McCammon (1983).

The IPC X-ray data were analyzed following the standard procedure described in Elvis et al. (1986) and Wilkes & Elvis (1987). Briefly, counts in the energy range ~ 0.15–3.5 keV were

Send offprint requests to: J.-L. Masnou
* Visiting Scientist, Harvard-Smithsonian Center for Astrophysics, Cambridge, Mass., USA
** Visiting Scientist, UPR176, DARC, Observatoire de Paris, Section de Meudon, France
*** Now at Marshall Space Flight Center, Huntsville, USA
**** Also Astronomy Program, University of Maryland, USA

Table 1. Observational details

Name	Redshift N_H[a]	I/MPC	Seq. No.	Date	Net counts[b]	T_{exp} (s)
0026+129	0.142	IPC	5417[c]	1981 Jan. 4	2678±55	11152
PG	4.93	MPC	518	1979 Jan. 7	1279±265	2826
0054+145	0.171	IPC	5418	1980 July 19	1289±39	11735
PHL 909	4.20	IPC	4248	1979 July 2	424±23	3717
0205+024	0.155	IPC	3978	1979 July 20	1237±38	7608
NAB	2.99					
0637−752	0.656	IPC	8494	1980 Dec. 14	1199±39	7480
PKS	8.4[d]	MPC	5404	1979 Nov. 30	546±138	860
1028+313	0.177	IPC	4256	1979 May 24	1167±37	6595
B2	1.98	MPC	4256[e]		561±275	3768
1219+756	0.07	IPC	5424	1980 Apr. 20	6434±107	13113
MKN 205	2.74	MPC	5424		8399±543	11305
1226+023	0.158	IPC	2037	1979 June 20	4523±68	1740
3C273	1.80[f]	MPC	2037		4015±152	737
		IPC	5692	1980 Jan. 1	9362±98	3911
		MPC	5692		16297±379	3482
		IPC	9310	1980 Dec. 13	6687±83	1668
1253−055	0.538	IPC	4645	1980 July 14	3279±65	25095
3C279	2.22	MPC	4645		1775±604	14828
1426+015	0.086	IPC	5348[g]	1980 Aug. 3	1231±36	2034
PG	2.64	MPC	5348		1585±210	1925
		IPC	10374[h]	1981 Jan. 5	4748±91	13210
1501+106	0.036	IPC	6713	1980 Jan. 18	1663±42	1475
MKN 841	2.23	MPC	6713		1153±155	1024
1613+658	0.129	IPC	10375[i]	1981 Feb. 6	2217±51	7209
PG	2.66					
2130+099	0.061	IPC	1972	1981 Apr. 20	862±33	4987
II Zw 136	4.20	IPC	1971	1980 May 3	485±23	1429
2135−148	0.20	IPC	5426	1980 May 10	2521±54	12902
PHL 1657	4.45	MPC	5426		2637±464	8560

[a] Galactic equivalent hydrogen column density in units of 10^{20} atoms cm^{-2} from Elvis et al. (1989) (unless otherwise noted)
[b] 0.15–3.5 keV (IPC, bin 1 excluded) and 2–10 keV (MPC, bins 1 to 6)
[c] Sum of sequence numbers 5417, 9550, 9551, 9552, 9553
[d] Heiles & Cleary (1979)
[e] Excluding bins 1, 2 due to their low counts
[f] Dickey et al. (1978)
[g] Spectral results reported by Elvis et al. (1986)
[h] Sum of sequence numbers: 10374, 10390, 10391, 10392, 10393
[i] Sum of sequence numbers: 10375, 10394, 10395, 10396, 10397

obtained from a 3′ circle centered on the position of the source. A correction was applied for counts falling outside this circle and background counts were estimated from a 5′–6′ annulus centered on the source position. The first bin of the pulse height distribution was excluded since the errors are not well determined.

In this new analysis we have also used data from the MPC for which >500 net counts were detected. Apart from the early studies by Halpern (1981) and Elvis et al. (1986), the MPC has been little used for quasars until now due to systematic uncertainties in the background subtraction process for these faint

Table 2. Fits to 3C273 **a** Wilkes & Elvis (1987) style, single power law fits (1σ error bars); **b** Comparison of single power law fits to MPC only and IPC/MPC

a

Seq. no.	PH channels	α_E	N_H (10^{20} atoms cm^{-2})	χ^2_{min}/d.o.f[a]	f(1.0 keV)[b]
5692	2–11	$0.34^{+0.09}_{-0.07}$	$0.3^{+0.4}_{-0.3}$	10.7/8	9.4 ± 1.1
9310	2–9	$0.46^{+0.11}_{-0.11}$	$1.0^{+0.6}_{-0.6}$	6.3/6	18.7 ± 3.0

b

Seq. No.	MPC α_E	MPC $f_{1\,keV}$[b]	α_E(IPC/MPC)	$f_{1\,keV}$[b](IPC/MPC)
2037	0.42 ± 0.09	10.8 ± 1.3	0.55 ± 0.02	12.6 ± 0.2
5692	0.43 ± 0.05	9.4 ± 0.6	0.62 ± 0.02	11.3 ± 0.1

[a] Degrees of freedom

[b] Normalization in μJy, errors are quoted at 1σ for one interesting parameter

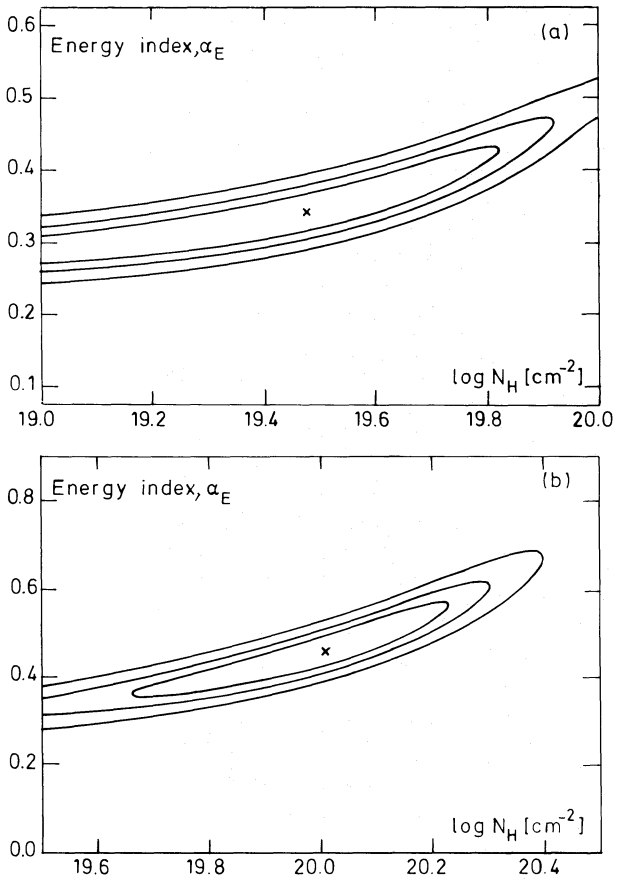

Fig. 1a and b. 68%, 90% and 99% confidence contours for α_E and N_H for single power law [Wilkes & Elvis (1987) style] fits to observations of 3C273, sequence numbers: **a** 5692 and **b** 9310. These are included for comparison with the earlier results

sources. These uncertainties have now been reduced and quantified for all observations prior to October 1980 (Arnaud 1991 and see below) allowing simultaneous fitting of IPC and MPC data.

The MPC data have the advantage of covering a higher energy range, with the counts distributed into 8 pulse height channels extending from 1.2 to 20 keV. Channels 7 and 8 (>10 keV) were not used in this analysis as they provide no additional constraint on the spectral fits. The energy range of our study generally covers the two decades 0.1–10 keV. In most cases the MPC and IPC data were obtained simultaneously. The exceptions are PG 0026+129, II Zw 136 and PKS 0637−752 where no significant variation was detected between the two dates and nonsimultaneous data were used to maximize the signal-to-noise ratio.

2.2. *The monitor proportional counter (MPC)*

The MPC was a collimated proportional counter filled with argon and sealed with a 38 μm window of beryllium foil. Its effective area was 667 cm^2 with a triangular field of view having full width at half maximum of 43′ and a flattened top ~6′ wide. Counts were collected in 8 pulse height (PH) channels from 1.2–20 keV, with an energy resolution of ~20% at 6 keV. The instrument was mounted on the outside of the Einstein Observatory telescope and aligned within 1′ of the optical axis. The MPC is described in detail by Gaillardetz et al. (1978) and Grindlay et al. (1980).

We used the latest, Rev1, time-ordered MPC processing with data extracted following the method of Arnaud (1991). Briefly, all data taken during points in the orbit with McIlwain $l > 1.2$, $B < 0.25$, which includes the South Atlantic Anomaly passage, were discarded. The background consists of two components. A background model for the cosmic background was constructed using source-free observations. The background is estimated using correlations with the pulse risetime discriminator rates and McIlwain l, B, parameters modified by long-term time variability which includes the decay of the in-flight calibration source (Cd^{109}), modeled as an exponential with a half-life of 450.4 days. In addition, the response matrix was modified following the discovery that the earlier, Rev0, processing system assumed an energy resolution ~10 times better than that in reality. The resulting effective area curve is shown by Vrtilek et al. (1990) and Arnaud (1991).

2.3. IPC/MPC relative normalization

The IPC and MPC instruments were calibrated independently and the estimated accuracy of these calibrations are about 10% and 20%, respectively. Before combining data from the IPC and MPC, the relative accuracy of their calibrations must be determined. Since the instruments have very different sensitivities they did not observe the same calibration sources. Instead, we made a comparison utilizing the quasar data under the assumption (consistent with Ginga results; Pounds 1990) that quasar spectra do not change drastically ($\Delta\alpha < 0.5$) in the 0.6–10 keV energy range.

A single power law model, with the line-of-sight absorbing column density fixed at the Galactic value, was fitted to the high-energy band of the IPC (0.6–3.5 keV) to minimize the effects of any soft excess. A power law model with the IPC best-fit slope and Galactic N_H was then fitted to the MPC data but with the normalization (flux density at 1 keV) free. These fits should give comparable normalization in both instruments. In all but the highest S/N observations, those of 3C273, the ratio of MPC to IPC normalization (Fig. 2) is consistent with unity. However, a weighted mean gives a value of IPC/MPC = 1.14 ± 0.04, similar to those for 3C273 and implying that the MPC calibration is too low relative to the IPC. This conclusion is reinforced by a comparison of the best-fit power law slopes determined by fitting the IPC and MPC data individually and in combination for the two 3C273 observations where this is possible (Table 2b and Wilkes & Elvis 1987). The IPC/MPC combination gives a steeper slope ($\alpha_E \sim 0.6$) than either instrument individually, which each gave $\alpha_E \sim 0.4$. The latter is in better agreement with measurements of 3C273 by other experiments (Worrall et al. 1979; Turner et al. 1990a, b). Since the ratio of IPC to MPC normalization is not sensitive to the spectral slope assumed, our result does not critically depend on the accuracy of the spectral fit.

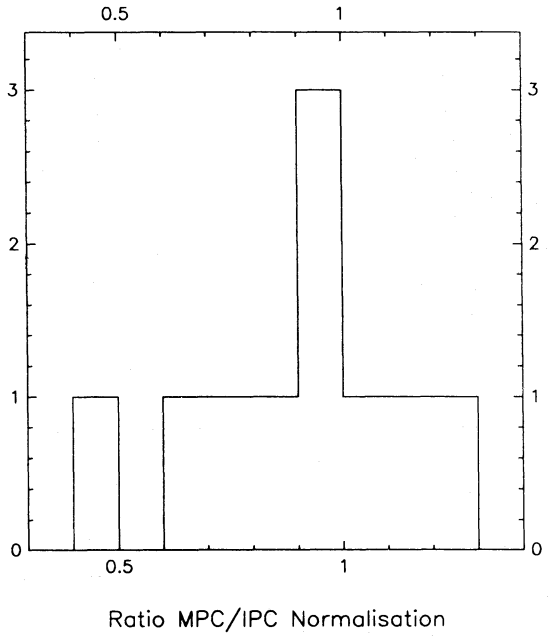

Fig. 2. A histogram of IPC relative to MPC normalization for single power law fits using the IPC best-fitted slope

We conclude that the relative normalization of the MPC is systematically low relative to the IPC by a factor of 1.14. This is within the absolute accuracy of the calibration of each instrument. The MPC data were corrected accordingly in our subsequent analysis and all numbers presented here include this correction. We note that the decision of which instrument to correct is arbitrary.

2.4. Spectral analysis

The results of conventional, single power law models, with N_H fixed at the Galactic value, are presented in Table 3. They are poor [$P(\chi^2) \leq 10\%$] for 9 observations of 7 of the 13 quasars analyzed here. In 11 observations the residuals clearly show the lowest 1 or 2 PHA (pulse height analysis) channels to be significantly above the fit, suggesting the presence of a soft excess.

Conventional two-component fits give poorly constrained parameters [slope and normalization at 1.0 keV, f(1.0 keV)] for the low-energy excess (e.g. Arnaud et al. 1985; Pounds et al. 1986). However, the excess flux can be much better determined than its spectrum since a small change in flux at 0.2 keV results in a large change in slope and normalization [f(1.0 keV)]. We have, therefore, applied broken power law fits to the data, minimizing χ^2 with respect to the 0.2 keV flux in each component and to the 1.0 keV flux of the high-energy component [f_{XS}(0.2 keV), f_{HE}(0.2 keV), f(1.0 keV), respectively] instead of the more conventional spectral slope. The results are given in Fig. 3 and Table 3, with errors quoted at 1σ for one interesting parameter, $\Delta\chi^2 = 1.0$ (Avni 1976). N_H was again fixed at the Galactic value. The energy resolution and S/N of the data are insufficient to warrant the addition of a fourth free parameter; thus, it is not possible to determine the break energy between the two power laws. The IPC is best suited to detecting soft excesses in its lowest independent energy band, i.e. with break energy in the range 0.4–0.6 keV. The break energy was thus fixed at 0.6 keV, yielding a conservative estimate of the observed flux in any detected excess. Decreasing this value to 0.4 typically results in a small but insignificant ($< 2\sigma$) increase in the deduced flux of the soft excess.

Fits with power law plus backbody components were also applied, leaving free the 0.2 keV flux in each component and the normalization of the high-energy component. The energy resolution is not sufficient to fit the blackbody temperature, which was therefore fixed at 0.05 keV. Both the high-energy component and the soft excess flux are consistent with corresponding results from the broken power law fits as shown in Fig. 4. Our discussion will be confined to the results of the broken power law model.

An F-test for the significance of an additional parameter shows that a broken power law model represents a significant improvement over a single power law fit for 8 of the 16 observations (5 of the 10 with MPC data) at 5% (0.05) confidence or better (Table 3). Including PG 1211 + 143, this leads to a total of 9 excesses detected in observations of 8 quasars from our sample of 14. Upper limits at 3σ are given for the remaining 8 observations for which no significant excess was detected.

2.5. The effect of additional absorption

The presence of any additional absorbing material (molecular and partially ionized Galactic or material intrinsic to the quasar) along the line of sight to a quasar would increase the requirement

Table 3. Parameters of spectral fits

Name	IPC MPC	Single power law α_E	Single power law $f(1.0\text{ keV})^a$	Single power law χ^2 Bins	Broken power law $f(1.0\text{ keV})^a$	Broken power law f_{HE} (0.2 keV)^b	Broken power law f_{XS} (0.2 keV)^c	Broken power law $\alpha_{HE}{}^d$ $\alpha_{LE}{}^d$	Broken power law χ^2 Bins	Sig^e
0026+129	I5417	0.88 ± 0.05	1.41 ± 0.03	10.0	$1.41^{+0.07}_{-0.07}$	$5.9^{+1.4}_{-1.1}$	<13.5	0.88	10.0	—
PG	M518			14				0.87	14	
0054+145	I5418	0.74 ± 0.07	0.61 ± 0.02	18.8	$0.52^{+0.04}_{-0.04}$	$1.02^{+0.33}_{-0.26}$	$4.16^{+1.63}_{-1.58}$	0.41	11.5	0.01
PHL 909	14248			21				1.89	21	
0205+024	I3978	1.80 ± 0.07	0.70 ± 0.03	14.6	$0.58^{+0.06}_{-0.06}$	$4.0^{+2.4}_{-1.5}$	$14.8^{+4.4}_{-5.0}$	1.2	8.4	0.05
NAB				11				2.61	11	
0637−752[f]	I8494	0.46 ± 0.10	0.98 ± 0.05	6.4	$0.97^{+0.05}_{-0.09}$	$2.0^{+0.5}_{-0.5}$	<32.8	0.44	6.4	—
PKS	M5404			15				0.97	15	
1028+313	I4256	0.96 ± 0.06	0.91 ± 0.03	9.4	$0.76^{+0.07}_{-0.07}$	$2.1^{+0.5}_{-0.5}$	$5.4^{+2.0}_{-2.1}$	0.62	3.8	0.01
B2	M4256			12				1.79	12	
1219+756	I5424	0.96 ± 0.03	2.49 ± 0.04	25.9	$2.24^{+0.08}_{-0.08}$	$7.8^{+1.0}_{-0.9}$	$8.9^{+2.4}_{-2.5}$	0.78	14.3	0.01
MKN 205	M5424			16				1.47	16	
1226+023	I2037	0.55 ± 0.02	12.6 ± 0.2	23.6	$11.8^{+0.4}_{-0.4}$	$25.0^{+2.1}_{-2.0}$	$16.6^{+6.0}_{-6.0}$	0.47	16.0	0.05
3C273	M2037			15				0.93	15	
	I5692	0.62 ± 0.01	11.3 ± 0.1	83.3	$9.8^{+0.2}_{-0.2}$	$20.1^{+1.1}_{-1.1}$	$28.8^{+3.3}_{-3.3}$	0.45	14.5	0.01
	M5692			16				1.26	16	
	I9310	0.63 ± 0.03	20.2 ± 0.3	10.6	$18.9^{+0.7}_{-0.7}$	$41.5^{+6.1}_{-5.4}$	<71.2	0.49	5.6	—
				8				1.00	8	
1253−055	I4645	0.62 ± 0.04	0.63 ± 0.01	27.0	$0.67^{+0.02}_{-0.04}$	$2.2^{+0.2}_{-0.5}$	<1.8	0.74	26.1	—
3C279	M4645			16				0.29	16	
1426+015	I5348	1.19 ± 0.05	3.05 ± 0.09	16.8	$2.94^{+0.2}_{-0.2}$	$17.9^{+5.9}_{-4.7}$	<32.5	1.12	16.5	—
PG	M5348			15				1.37	15	
	I10374	1.16 ± 0.04	1.91 ± 0.04	11.4	$1.73^{+0.09}_{-0.09}$	$7.8^{+2.0}_{-1.6}$	<21.3	0.94	7.2	—
				8				1.65	8	
1501+106	I6713	1.27 ± 0.04	4.82 ± 0.14	15.2	$4.2^{+0.3}_{-0.3}$	$18.7^{+5.0}_{-4.0}$	$30.6^{+8.3}_{-9.3}$	0.93	7.1	0.01
MKN 841	M6713			16				1.82	16	
1613+658	I10375	1.21 ± 0.04	1.40 ± 0.04	7.0	$1.33^{+0.07}_{-0.07}$	$7.9^{+2.4}_{-1.8}$	<12.4	1.10	6.3	—
PG				11				1.39	11	
2130+099	I1971	1.41 ± 0.07	1.14 ± 0.04	14.7	$0.91^{+0.08}_{-0.08}$	$3.4^{+1.5}_{-1.1}$	$19.4^{+5.4}_{-5.3}$	0.81	3.2	0.01
II Zw 136	I1972			10				2.55	10	
2135−148	I5426	0.73 ± 0.05	1.10 ± 0.02	24.6	$1.10^{+0.05}_{-0.05}$	$3.4^{+0.5}_{-0.5}$	<6.3	0.71	24.6	—
PHL 1657	M5426			16				0.81	16	

[a] Normalization in μJy. Errors are quoted at 1σ for one interesting parameter

[b] Flux density of high-energy component at 0.2 keV (observed frame) in μJy, corrected for Galactic absorption

[c] Flux density in excess at 0.2 keV (observed frame) in μJy, corrected for Galactic absorption. Upper limits are at 3σ

[d] α_{HE}, α_{LE}: high- and low-energy power law energy indices, respectively, resulting from the fitted X-ray fluxes

[e] Significance of the soft X-ray excess as determined by an F-test

[f] 0637–752 has no accurate Galactic N_H measurement due to its southern declination. Fits were performed at the Galactic value $\pm1\ 10^{20}$ and no evidence for a soft excess was found in either case

for a soft excess. We have quantified this effect for the case of partially ionized hydrogen in the Galaxy. Reynolds (1989) estimated that 37% of the gas along a high-latitude line of sight through the Galaxy is ionized. Increasing the metal contribution to our X-ray opacities by 37% results in the detection of 4 more excesses for 3 quasars: [3C273 (9310), 1426+015 (both observations) and 1613+658]. For those quasars with a detected excess, the 0.2 keV flux of the excess increased by 20–43%.

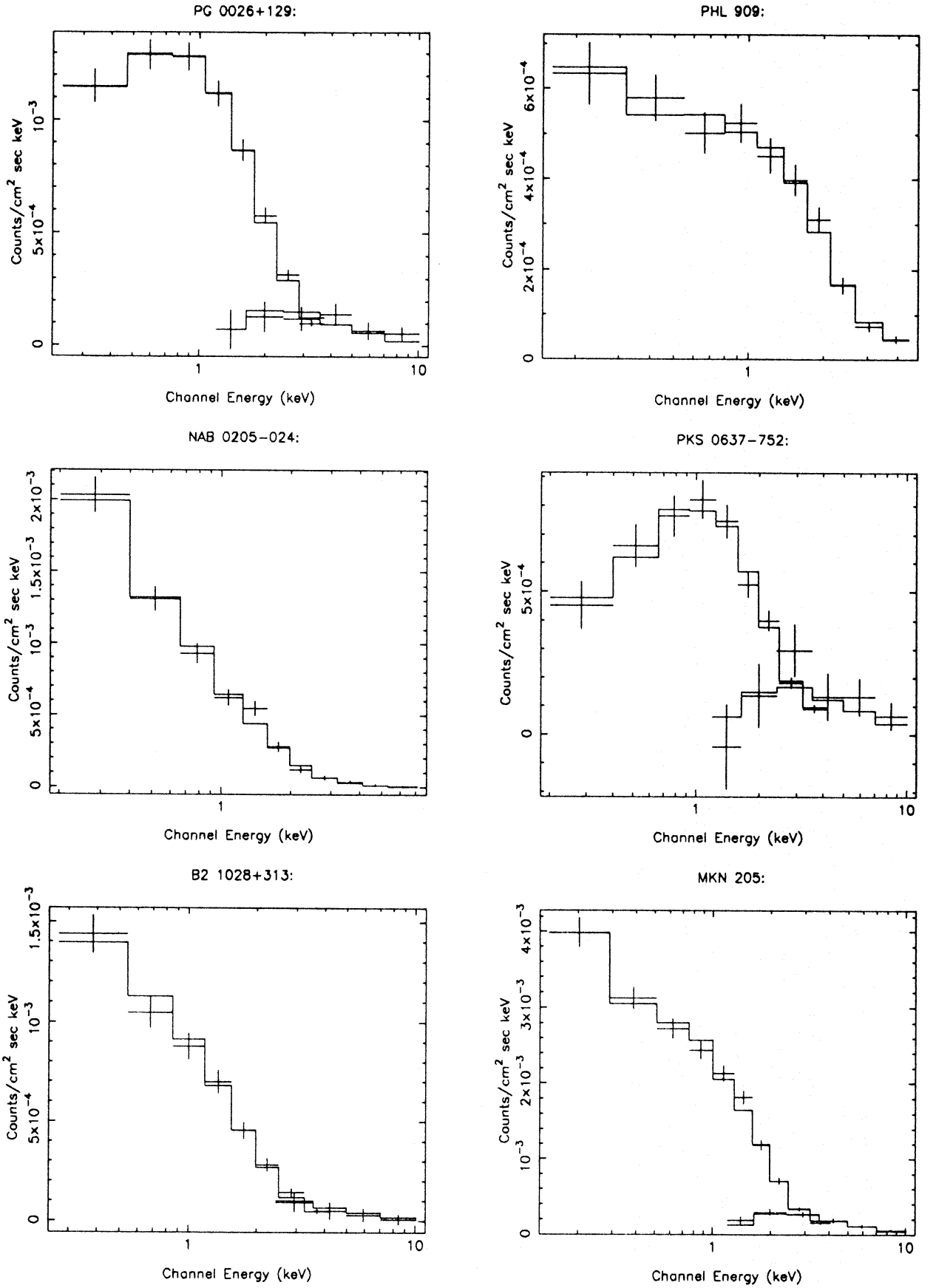

Fig. 3. Results of broken power law fits to the IPC plus MPC data

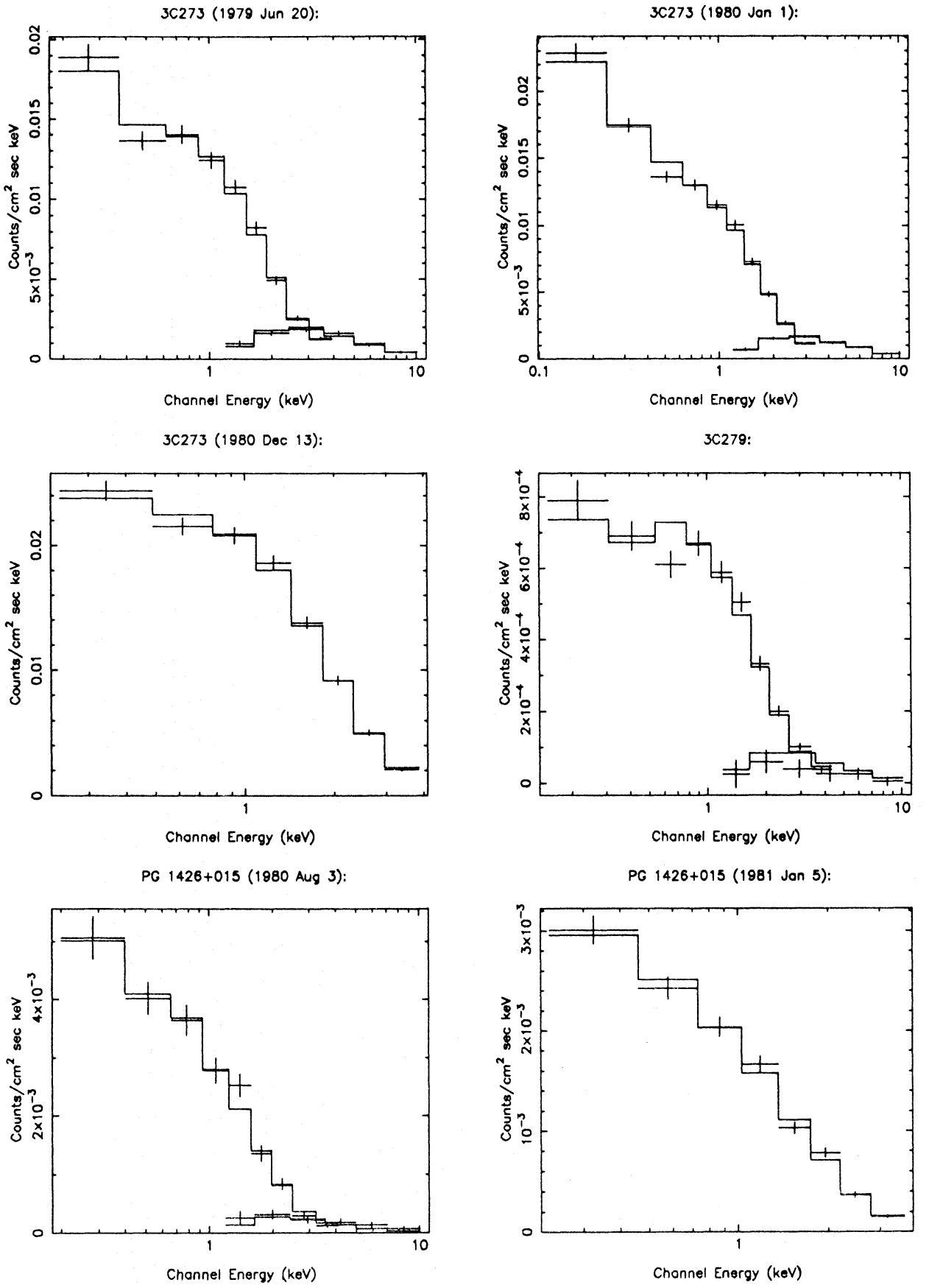

Fig. 3 (continued)

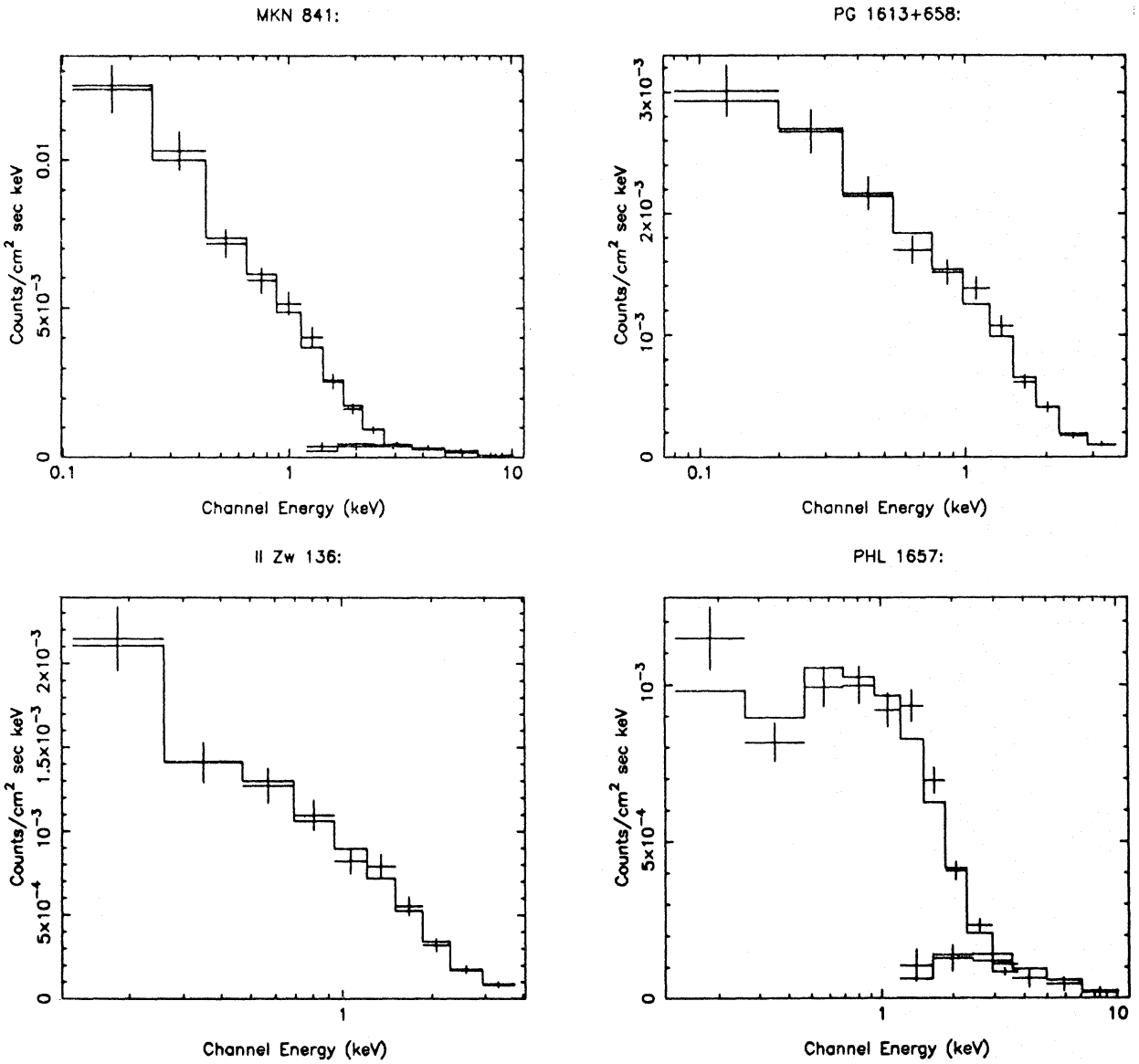

Fig. 3 (continued)

2.6. Notes on individual objects

2.6.1. PG 1211+143

PG 1211+143 is already known to have a steep low-energy spectrum (Elvis et al. 1985; Bechtold et al. 1986; Czerny & Elvis 1987). This soft excess is unusual since it is reported to display a break energy around 2 keV, much higher than the 0.3–0.6 keV generally seen. The MPC data for this object are unreliable, as are all MPC observations made after October 1980, due to a change in instrument configuration on that date[1]. The lack of higher-energy data combined with the 2 keV break energy between the excess and the high-energy component make it impossible to constrain the spectral parameters and so it is not analyzed here. Since it is a part of the sample, we include it in our discussion. A detailed discussion of its spectrum both from Einstein and EXOSAT data is given by Elvis et al. (1991b) and from Ginga data by Turner et al. (1990a).

2.6.2. 3C273

There are three observations of 3C273 over 17 months. The first observation has a weak excess (Table 3). In the second, 6 months later, the excess has almost twice the flux level of the first and in the third, 11 months later than the second, the upper limit is consistent with both the earlier measurements. The high-energy flux density also varies but is uncorrelated with a 20% decrease over 6 months followed by a 93% increase over 11 months. Similar, uncorrelated low and high variations were found in Ginga and EXOSAT observations of 3C273 (Turner et al. 1990b).

2.6.3. PHL 1657 (2135−148)

The X-ray spectrum is not fitted well by a power law or a blackbody form. A good fit was obtained with a partial covering

[1] This change in state of the MPC was not known at the time of the earlier IPC/MPC study by Bechtold et al. (1986).

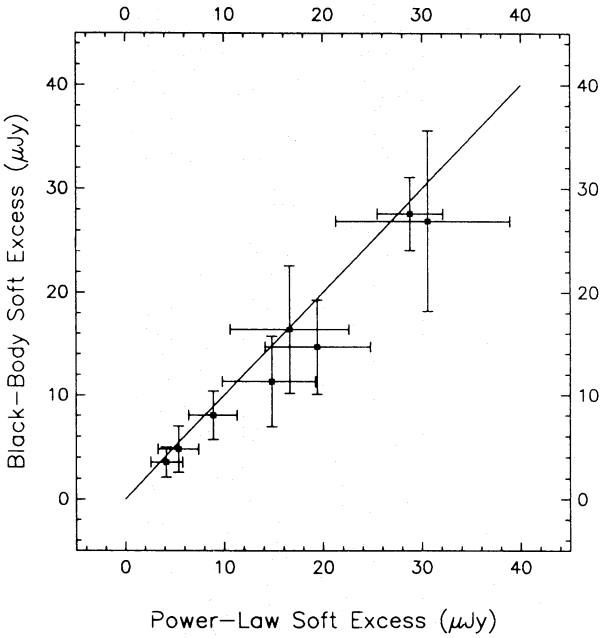

Fig. 4. Comparison of the 0.2 keV flux density in the soft excess component as determined using a power law and a blackbody as the spectral form for the soft component

model (see e.g. Turner & Pounds 1989): $\alpha_E = 2.1 \pm 0.5$, N_H (additional) $= 7.1 \pm 1.6\ 10^{20}$ cm^{-2} (fraction $92 \pm 7\%$), $f(1.0\ \text{keV}) = 4.1 \pm 1.6$ μJy ($\chi^2 = 15$, $n = 16$).

Optical images of this source show two nearby companions and surrounding nebulosity (Hutchings et al. 1984) extending to $> 6''$ so that additional X-ray absorption is likely to be present. X-ray spatial structure at this level cannot be confirmed at the resolution of the IPC and, indeed, the IPC image shows no evidence for extended emission. There is a possibility that the closest companion, a fainter quasar at the same redshift only 1'.9 away, may contribute to the X-ray flux leading to the complex spectrum. Two, higher energy, EXOSAT observations of this quasar show no evidence for a complex spectrum. A single power law fit gives an energy spectral index ~ 0.7 (Singh et al. 1991). However, these authors also report a variation in the (0.2–1.0 keV) soft X-ray flux during this time, which might indicate complexity at lower energies.

2.7. *Excess above an IR–X-ray baseline*

Under the hypothesis that the soft X-ray excess is the high-energy tail of the blue bump, we would expect its flux to correlate with the strength of the blue bump. However, the soft X-ray excess is measured with respect to the higher-energy X-ray power law while the blue bump is generally estimated relative to the IR emission. While it has been suggested that the IR and X-ray emission is related (Malkan 1984; Carleton et al. 1987), it is by no means proven and the lack of any relation could invalidate a search for a blue bump/soft excess correlation due to the large continuum range involved. Alternatively, both components could be measured above the common baseline of an effective IR/X-ray power law. We have, therefore, estimated the soft X-ray excess above this power law as a check on our earlier results.

An estimate of the spectral slope from IR to X-ray was made from luminosities integrated between 1–2 μm and 0.6 keV using data from Elvis et al. (1991c, and Fig. 8), with the exception of 1253 − 055 (3C279) for which we have little multiwavelength data. The monochromatic luminosity at 0.2 keV in the rest frame, for a soft X-ray excess above the IR–X-ray power law was computed. Such an excess is present at $> 1\sigma$ for 7 of the 8 quasars which show an excess above the high-energy X-ray power law. One quasar, 3C273, no longer shows an excess. The fitted results for all 7 objects and upper limits for the remainder are given in Table 4.

3. Results

3.1. *Soft excess above the high-energy X-ray power law*

The flux density in the soft X-ray excess at 0.2 keV ranges from ~ 1–6 times that in the high-energy component at the same energy (Table 4). It is clearly very strong, dominating the energy output in the soft X-ray region ($\lesssim 0.3$ keV) in quasars.

The soft excess was detected, at $\gtrsim 90\%$ confidence, in 7 of the 13 quasars analyzed here and also in PG 1211 + 143. Five of these were reported by Wilkes & Elvis (1987), the remaining two, NAB 0205 + 024 and B2 1028 + 313, are new detections in this analysis. Including PG 1211 + 143, this yields 8 of 14 quasars with an excess. Studies of lower luminosity Seyfert 1 galaxies (Turner & Pounds 1989; Kruper et al. 1990) show a similar $\sim 50\%$ detection rate. This number is likely to increase if, as discussed above, a significant fraction of the hydrogen in our galaxy is ionized (Reynolds 1989). Our results confirm that soft excess components are common in many types of active galaxies and over a wide range in luminosity.

3.2. *Soft excess above an IR–X-ray baseline*

When measured relative to an IR–X-ray power law, 7 of the 8 quasars earlier found to have an excess still have one at $> 1\sigma$ (Table 4). 3C273 is the exception, leaving 1 radio-loud and 6 radio-quiet quasars with soft X-ray excesses. Figure 5 shows the

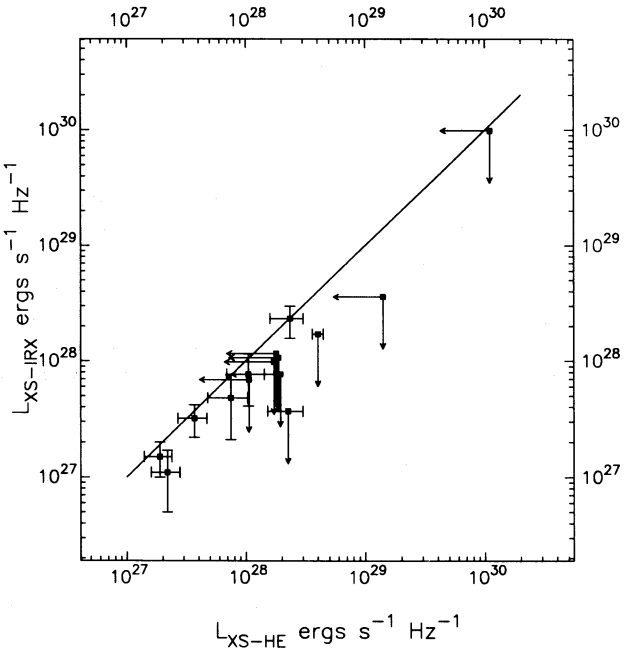

Fig. 5. Comparison of the soft X-ray excess determined relative to the high-energy X-ray power law and the IR–X-ray power law

Table 4. Luminosity of the excess

Name	IPC MPC	$f_{XS}(0.2)/f_{HE}(0.2)$[a]	α_{IRX}[b]	L[c] 1 keV	L_{XS-HE}[d] 0.2 keV	L_{XS-IRX}[e] 0.2 keV	CE87[f] ratio	R_L[g] f_{BB}[h]
0026+129	I5417	<2.3	1.17	0.14	<1.88	<1.07		0.34
PG	M518							4.7
0054+145	I5418	$4.1^{+1.9}_{-2.0}$	1.33	0.07	$0.75^{+0.28}_{-0.27}$	$0.48^{+0.28}_{-0.27}$	3.76	−0.01
PHL 909	I4248							2.3
0205+024	I3978	$3.7^{+1.8}_{-2.6}$	1.24	0.07	$2.35^{+0.67}_{-0.76}$	$2.33^{+0.67}_{-0.76}$	5.87	−0.40
NAB								6.7
0637−752	I8494	<16.3	1.14	2.35	<110	<98.6		3.52
PKS	M5404							8.0
1028+313	I4256	$2.6^{+0.9}_{-0.9}$	1.17	0.11	$1.05^{+0.38}_{-0.36}$	$0.77^{+0.38}_{-0.36}$	42.6	2.14
B2	M4256							4.7
1219+756	I5424	$1.1^{+0.3}_{-0.4}$	1.19	0.05	$0.22^{+0.06}_{-0.06}$	$0.11^{+0.06}_{-0.06}$	2.5	−0.31
MKN 205	M5424							1.6
1226+023	I2037	$0.7^{+0.3}_{-0.3}$	1.21	1.36	$2.26^{+0.74}_{-0.74}$	$-1.85^{+0.74}_{-0.74}$	−0.36	3.06
3C273	M2037							5.7
	I5692	$1.4^{+0.2}_{-0.2}$	1.24	1.13	$4.03^{+0.43}_{-0.43}$	$0.42^{+0.43}_{-0.43}$	0.08	
	M5692							
	I9310	<1.7	1.15	2.19	<14.1	<3.6		
1426±015	I5348	<1.8	1.13	0.10	<1.80	<1.16		−0.55
PG	M5348							6.4
	I10374	<2.7	1.21	0.06	<1.06	<0.69		
1510+106	I6713	$1.6^{+0.6}_{-0.7}$	1.18	0.02	$0.19^{+0.05}_{-0.05}$	$0.15^{+0.05}_{-0.05}$	3.4	−0.67
MKN 841	M6713							3.9
1613+658	I10375	<1.6	1.21	0.11	<1.72	<0.98		−0.10
PG								3.3
2130+099	I1971	$5.7^{+3.9}_{-3.0}$	1.35	0.02	$0.37^{+0.10}_{-0.10}$	$0.32^{+0.10}_{-0.10}$	2.40	0.37
II Zw 136	I1972							6.0
2135−148	I5426	<1.9	1.18	0.22	<1.95	<0.77		1.70
PHL 1657	M5426							2.4

[a] Ratio of excess and high-energy X-ray power law contributions at 0.2 keV. Upper limits are at 3σ and errors at 1σ for one interesting parameter

[b] Index of the power law connecting the infrared (1–2 μm) flux to the X-ray flux at 0.6 keV

[c] Luminosity of the high-energy power law component at 1 keV in units of 10^{28} erg s^{-1} Hz^{-1} ($H_0 = 50$ km s^{-1} Mpc^{-1}, $q_0 = 0$)

[d] Luminosity of the excess value above the high-energy X-ray power law in units of 10^{28} erg s^{-1} Hz^{-1}. The upper limits are at 3σ and errors at 1σ for one interesting parameter

[e] Luminosity of the excess observed above the IR–X-ray power law connecting the infrared (1–2 μm) to the X-ray spectrum at 0.6 keV in units of 10^{28} erg s^{-1} Hz^{-1}. The upper limits are at 3σ and errors at 1σ for one interesting parameter

[f] EL (0.2 keV)/$EL(10^{15}$ Hz), see Sect. 3.6

[g] Radio-loudness (Wiles & Elvis 1987)

[h] Ratio of blue bump to IR–X-ray power law in the range 0.1–0.2 μm

comparison of the excess determined by the two methods with the line of equality shown. With the exception of 3C273, the soft excesses determined according to the two different methods agree. Although insignificant, the sense of any difference is that the excess strength decreases when measured with respect to the IR–X-ray power. This implies that the IR–X-ray slope is generally steeper than the high-energy X-ray power law (see Tables 3, 4).

A decrease in the apparent strength of the soft X-ray excess when it is measured relative to an IR–X-ray power law is expected for radio-loud objects such as 3C273. They are stronger X-ray

sources than their radio-quiet counterparts; this is thought to be due to the presence of an additional, radio-linked, high-energy, X-ray component (Zamorani et al. 1981; Wilkes & Elvis 1987). This picture also predicts smaller IR–X-ray power law slopes for radio-loud quasars, although for our small sample the difference is only 2σ; $\alpha_{IRX} = 1.18 \pm 0.02$ (radio-loud), $= 1.22 \pm 0.02$ (radio-quiet).

3.3. *Relation to other properties*

The magnitude and errors of our detected flux densities at 0.2 keV suggest that a redshift of 0.5 would be sufficient to make it undetectable in most cases. The lack of a detected excess in the two highest redshift objects in our sample ($z > 0.5$), PKS 0637 −752 and 3C279, is consistent with this prediction.

In the current sample, 2 of the 5 radio-loud and 6 of the 9 radio-quiet quasars show excesses. The probability of seeing such a distribution if the parent populations of these two samples are the same is 28% (Fisher test), i.e. there is no evidence from this small sample that radio-loud and radio-quiet objects are different in either the presence or the strength of their excess properties. This conclusion does not change if we instead determine the soft excess above the IR–X-ray baseline. It is strengthened if we omit the two higher-redshift quasars which are borh radio-loud.

No relation was found between the soft X-ray excess, measured in either way, and the high-energy X-ray luminosity density (at 1.0 keV) (16% probability of a chance occurrence).

3.4. *The high-energy component*

Figure 6 shows a comparison of the high-energy slopes determined from the broken power law fits with those reported by Wilkes & Elvis (1987) for a single power law fit with free N_H. The results are consistent in all cases, confirming the Wilkes & Elvis (1987) conclusion that allowing free N_H in a single power law fit with the IPC successfully models the soft X-ray excess. We confirm and extend their primary result that a range of slopes is present in the soft X-ray region, 0.2–10 keV, with the slopes for radio-loud and radio-quiet quasars being $\alpha_E \sim 0.5$, 1.0, respectively.

A synchrotron self-Compton origin for the $\alpha_E \sim 0.5$ X-ray component in radio-loud quasars is generally accepted (Zamorani et al. 1981; Wilkes & Elvis 1987). For radio-quiet quasars and Seyfert 1 galaxies, the currently popular reflection model, in which the X-rays are reflected off cool, optically thick, matter surrounding the central continuum source (Lightman & White 1988; Guilbert & Rees 1988), nicely explains all the available X-ray spectra. The model predicts $\alpha_E \sim 1.0$ at low energies, $\lesssim 5$ keV, as seen for radio-quiet quasars with Einstein IPC (Table 3), and a broad hump of emission extending from ~ 10 keV to high energy (~ 300 keV). It was the detection of this hump by Ginga, for a sample of Seyfert 1 galaxies (see Pounds 1990 for a review), which first brought this model to the fore. The intermediate, $\alpha_E \sim 0.7$, 2–10 keV slope, frequently reported for Seyfert 1 galaxies by HEAO1-A2 (Mushotzky 1985) and EXOSAT (Turner & Pounds 1989), is the natural result of fitting a single power law to the complex spectrum predicted by the reflection model. Data for individual Seyfert 1 galaxies observed with both HEAO1-A2 and the Einstein IPC (0.2–3.5 keV) confirm this conclusion in that the HEAO1-A2 (~ 0.7) slopes are smaller than the IPC (~ 1.0, Kruper et al. 1990). Although we see no evidence for a reflection component in the current quasar sample, the S/N of the MPC data is so low that it is unlikely to be detected.

3.5. *Relation to the blue bump*

The far-infrared to X-ray energy distributions for those quasars with a soft excess are shown in Fig. 8. These distributions are corrected for Galactic reddening and emission lines have been

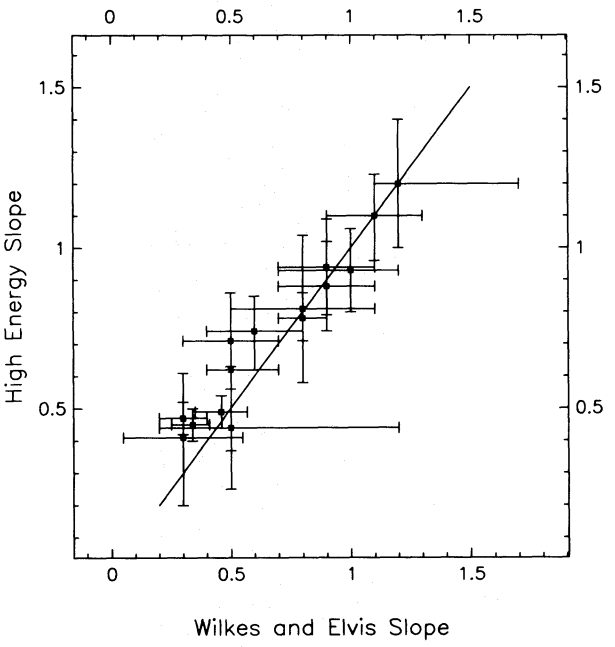

Fig. 6. Comparison of the IPC/MPC slopes determined here with the IPC alone results of Wilkes & Elvis (1987)

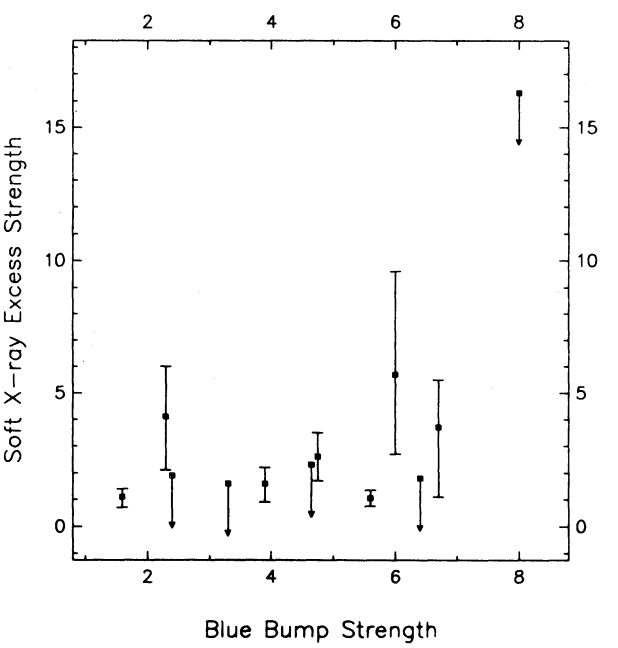

Fig. 7. The strength of the blue bump vs. that of the soft X-ray excess relative to the higher-energy X-ray power law

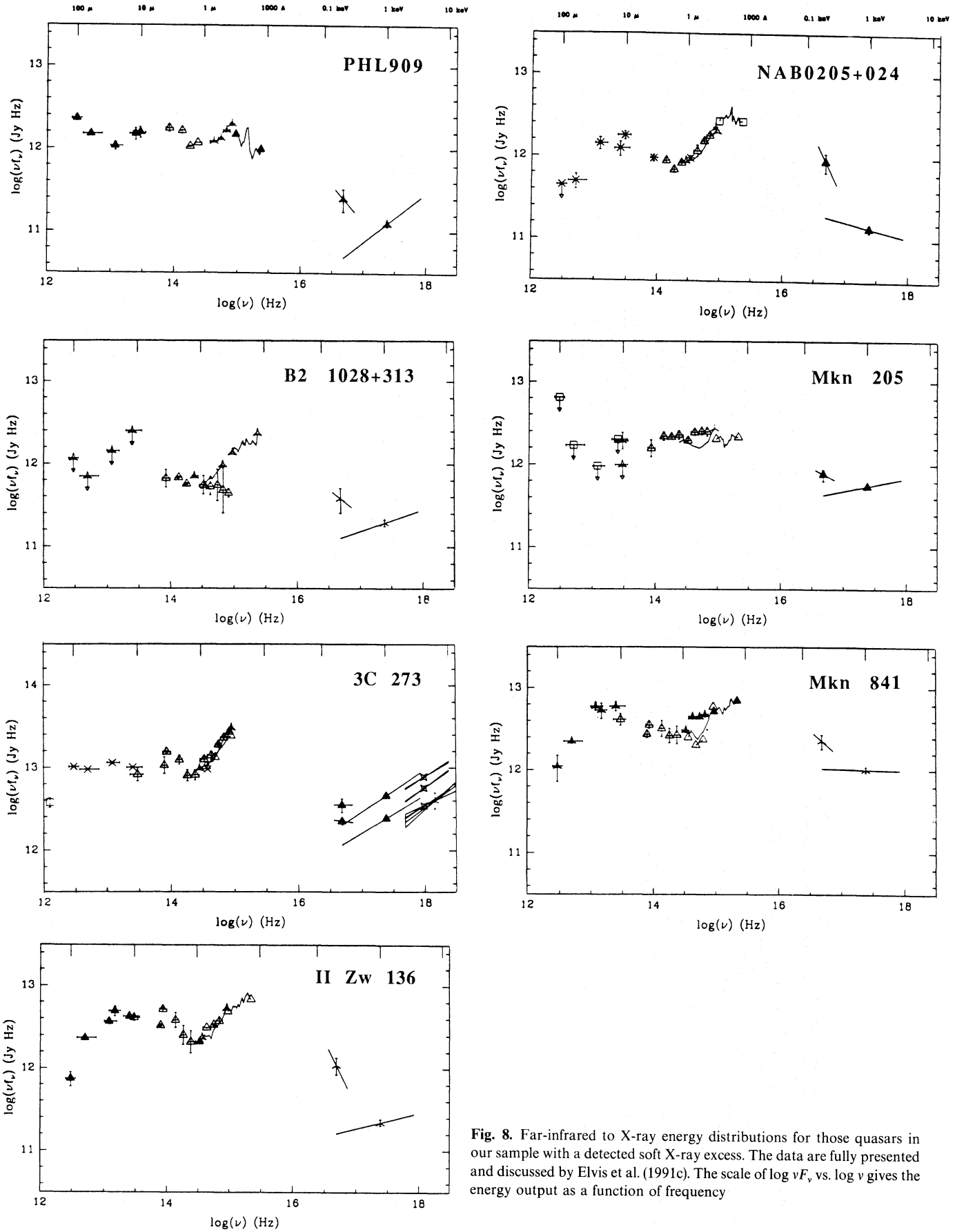

Fig. 8. Far-infrared to X-ray energy distributions for those quasars in our sample with a detected soft X-ray excess. The data are fully presented and discussed by Elvis et al. (1991c). The scale of log νF_ν vs. log ν gives the energy output as a function of frequency

subtracted. The data are being presented in detail by Elvis et al. (1991c) and so will be discussed no further here.

It is clear from the figures (e.g. NAB 0205+024) that the blue bump generally dominates the energy output of these quasars and that the soft X-ray excess may well be its high-energy tail. However, we found no evidence for a correlation between the strength of the blue bump (Fig. 7), as measured by the ratio of blue bump to IR–X-ray power law flux at 0.1–0.2 μm (f_{BB}),[2] and that of the excess, measured by its ratio to the high-energy component at 0.2 keV, [f_{XS}(0.2 keV)/f_{HE}(0.2 keV), Table 4]. This is true even when the two higher redshift (>0.5) objects are removed and when radio-loud and radio-quiet objects are considered separately. While this result is disappointing in view of the popular interpretation of the soft excess as the high-energy tail of the blue bump, it is clear from the figure that the uncertainties in the soft excess measurement are sufficiently large to mask any existing correlation. Further uncertainty is added by the possibility of variability and the possible presence of intrinsic, absorbing material.

No firm conclusions on the identity of the soft excess can be made until more data, in particular simultaneous UV and soft X-ray data with improved X-ray spectral resolution, have been obtained. This will be possible with ROSAT.

3.6. Comparison with the Czerny–Elvis model

Accretion disk models have generally not attempted to predict the soft X-ray flux in addition to the UV/optical regime, primarily due to the large uncertainties in the parameters of the inner regions of an accretion disk where this emission originates. Czerny & Elvis (1987) do include the soft X-ray and successfully reproduce the strong soft excess in PG 1211+143 using an electron scattering atmosphere surrounding the disk itself. In comparison with this result, column 8 ("CE87 ratio") in Table 4 gives the ratio (multiplied by 10) of the product energy–luminosity of the luminosity in excess of the IR–X-ray power law at 0.2 keV to that at 10^{15} Hz. This is similar to the parameter defined by Czerny & Elvis [1987, Eq. (28)]. They predict, assuming the accretion disk parameters for every quasar are the same and their inclinations are random, that ~15% of quasars will have observed values for this parameter >1.0. Six of the quasars with a soft X-ray excess, i.e. 40% of our sample, exceed this value implying that, for this model to apply, either the quasars in this sample are predominantly viewed face-on, or a range of model parameters is present.

4. Conclusions

Two-component spectral fits to IPC/MPC quasar data show that the soft X-ray excess dominates the X-ray flux $\lesssim$0.3 keV in half of our sample. The fluxes in the excess at 0.2 keV cover the range 1–6 times that in the high-energy component at the same energy. The lack of spectral information combined with uncertainty in the line-of-sight absorption makes it impossible to draw any definite conclusions concerning its identity. The high-energy tail of the blue bump remains the most attractive candidate and the common presence of both components, regardless of the class of AGN, might be considered as a circumstantial support for this picture. However, we cannot rule out such extreme alternatives as a completely new component or a single X-ray component which steepens below ~0.3 keV (Band & Grindlay 1986; Schwartz et al. 1990).

The high-energy slopes determined for the broken power law fits presented here are consistent with those reported earlier by Wilkes & Elvis (1987). Our results are fully consistent with the reflection model popularized by recent Ginga results for radio-quiet quasars and Seyfert 1 galaxies. For radio-loud quasars, the smaller ($\alpha_E \sim 0.5$) slope is consistent with the presence of a synchrotron self-Compton (SSC) radio-linked component (Zamorani et al. 1981; Wilkes & Elvis 1987), which probably dominates any reflection component in these quasars.

Measurements of the soft excess relative to an IR–X-ray power law agree well with those relative to the higher-energy X-ray in all objects except 3C273. This confirms that our soft excess measurements are valid for comparison with the blue bump flux which is measured with respect to the IR flux. Some weakening of the excess flux for radio-loud objects, such as 3C273, is consistent with their additional SSC component and stronger X-ray flux. Measurement with respect to the high-energy X-ray power law is the most sensitive way to detect the soft X-ray excess in radio-loud quasars. It is once again clear that radio-loud and radio-quiet quasars should be treated as distinct in X-ray studies.

Comparison of the observed ratio of the luminosity in excess of the IR–X-ray power law at 0.2 keV to that at 10^{15} Hz with that predicted by an accretion disk model, imply that a range of parameters is necessary to explain the whole sample. However, large uncertainties in line-of-sight absorption (Galactic or intrinsic to the quasar) and the lack of simultaneous UV data preclude detailed modeling. More, higher-resolution, soft X-ray observations (e.g. with ROSAT) are clearly necessary, preferably simultaneously with UV data, in order to delineate the blue bump unambiguously.

Acknowledgements. The authors thank Jules Halpern, Ken Pounds, Meg Urry and Saeqa Vrtilek for useful discussions. JLM thanks the High Energy Astrophysics Division, Harvard-Smithsonian Center for Astrophysics for their hospitality during short term visits for this work. BJW thanks her friends and colleagues at the Observatoire de Paris-Meudon for their kind hospitality and support during her visits. This research was partially supported by NASA grant NAS 8-30751. JLM and BJW acknowledge the support of the French Ministère des Affaires Etrangères. Mrs. Xenia Lasareff is acknowledged for the assistance in preparing the figures.

[2] This ratio is strongly correlated with the bump measure, C_{UV}/C_{IR}, McDowell et al. (1989), but is used in its place to be consistent with the X-ray measurement.

References

Arnaud K.A., 1991 (in preparation)
Arnaud K.A., Branduardi-Raymont G., Culhane J.L., Fabian A.C., Hazard C., McGlynn T.A., Shafer R.A., Tennant A.F., Ward M.J., 1985, MNRAS 217, 105
Avni Y., 1976, ApJ 210, 642
Band D.L., Grindlay J.E., 1986, ApJ 308, 576
Barvainis R., 1990, ApJ 353, 419
Bechtold J., Czerny B., Elvis M., Fabbiano G., Green R.F., 1986, ApJ 314, 699

Branduardi-Raymont G., Mason K.O., Murdin P.G., Martin C., 1985, MNRAS 216, 1043
Brown R.L., Gould R.J., 1970, Phys. Rev. D 2, 2252
Carleton N.P., Elvis M., Fabbiano G., Wilner S.P., Lawrence A., Ward M., 1987, ApJ 318, 595
Czerny B., Elvis M., 1987, ApJ 321, 305
Dickey J.M., Salpeter E.E., Terzian Y., 1978, ApJS 36, 77
Elvis M., Wilkes B.J., Tananbaum H., 1985, ApJ 292, 357
Elvis M., Green R.F., Bechtold J., Schmidt M., Neugebauer G., Soifer B.T., Matthews K., Fabbiano G., 1986, ApJ 310, 291
Elvis M., Lockman F.J., Wilkes B.J., 1989, AJ 97, 777
Elvis M., Wilkes B.J., McDowell J.C., 1991a, in: Berkeley Colloquium on Extreme Ultraviolet Astronomy, Malina R.F., Bowyer S. (eds), p. 238, Pergamon Press, New York
Elvis M., Giommi P., Wilkes B.J., McDowell J., 1991b, ApJ 378, 537
Elvis M., et al, 1991c, ApJS (in preparation)
Ferland G.F., Korista K.T., Peterson B.M., 1990, ApJ 363, L21
Gaillardetz R., Bjorkholm P., Mastronardi R., Vanderhill M., Howland D. 1978, IEEE Trans. on Nuc. Sci., NS-25, 437
Grindlay J.E., Marshall H.L., Hertz P., et al., 1980, ApJ 240, L121
Guilbert P.W., Rees M.J., 1988, MNRAS 233, 475
Halpern J., 1981, Ph.D. Thesis, Harvard University
Heiles C., Cleary M.N., 1979, Aust. J. Phys. Suppl. 47, 1
Hutchings J.B., Crampton D., Campbell B., Duncan D., Glandenning B., 1984, ApJS 55, 319
Kruper J.S., Urry C.M., Canizares C.R., 1990, ApJS 74, 347
Lightman A.P., White T.R., 1988, ApJ 335, 57
Malkan M., 1984, in: X-Ray and UV Emission from Active Galactic Nuclei, Brinkmann W., Trümper J. (eds), p. 121, MPE Report 184, October 1984. Max-Plank-Institut, Garching (R.F.A.)
Malkan M.A., Sargent W.L.W., 1982, ApJ 254, 22
McDowell J.C., Elvis M., Wilkes B.J., Willner S.P., Oey M.S., Polomski E., Bechtold J., Green R.F., 1989, ApJ 345, L13
Morrison R., McCammon D., 1983, ApJ 270, 119
Mushotzky R.F., 1985, Adv. Sp. Res. 3, 157
Pounds K.A., Stanger V.J., Turner T.J., King A.R., Czerny B., 1986, MNRAS 224, 443
Pounds K.A., 1990, in: Proceedings of the 23rd ESLAB Symposium on Two Topics in X-Ray Astronomy: 2 AGN and the X-Ray background, Hunt J., Battrick B. (eds), ESA-SP-296 (Vol. 2), p. 753, European Space Agency, Paris (France)
Reynolds R.J., 1989, ApJ 339, L29
Schwartz D.A., Qian Y., Tucker W., 1990, in: Proceedings of the 23rd ESLAB Symposium on Two Topics in X-Ray Astronomy: 2 AGN and the X-Ray background, Hunt J., Battrick B. (eds), ESA-SP-296 (Vol. 2), p. 1043, European Space Agency, Paris (France)
Shields G.A., 1978, Nat 272, 706
Singh K.P., Garmire G.P., Nousek J., 1985, ApJ 297, 333
Singh K.P., Rao A.R., Vahia M.N., 1991, A&A, 248, 37
Turner M.J.L., Williams O.R., Saxton R., Stewart G.C., Courvoisier T.J.-L. Ohashi T., Makishima K., Kli T., Inoue H., 1990a, in: Proceeding of the 23rd ESLAB Symposium on two Topics in X-Ray Astronomy: 2 AGN and the X-Ray background, Hunt J., Battrick B. (eds), ESA-SP-296 (Vol. 2), p. 769, European Space Agency, Paris (France)
Turner M.J.L., Williams O.R., Courvoisier T.J.L. et al., 1990b, MNRAS 244, 310
Turner T.J., Pounds K.A., 1989, MNRAS 240, 769
Vrtilek S.D., Mc Clintock J.E., Seward S.D., Kahn S.M., Wargelin B.J., 1991, ApJS 76, 1127
Wilkes B.J., Elvis M., 1987, ApJ 323, 243
Worrall D.M., Mushotzky R.F., Boldt E.A., Holt S.S., Serlemitsos P.J., 1979, ApJ 232, 683
Zamorani G., Henry J.P., Maccacaro T., Tananbaum H., Soltan A. et al., 1981, ApJ 245, 357